A Comparison of Semi-Lagrangian and Eulerian Polar Climate Simulations

DAVID L. WILLIAMSON AND JERRY G. OLSON

National Center for Atmospheric Research, Boulder, Colorado*

(Manuscript received 16 May 1997, in final form 25 August 1997)

ABSTRACT

The differences in the polar lower-troposphere temperature simulated by semi-Lagrangian and Eulerian approximations are examined and their cause is identified. With grids having 8–10 layers below 500 mb, semi-Lagrangian simulations are colder than Eulerian by 2–4 K in the region poleward of 60°N and below 400 mb in winter. Diagnostic calculations with the NCAR CCM3 show that the semi-Lagrangian dynamical approximations tend to produce a cooling relative to the Eulerian at the 860-mb grid level. The difference occurs over land and sea ice where an inversion forms in the atmosphere with its top at the 860-mb grid level. The source of the difference is shown to be the different way the vertical advection approximations treat vertical structures found at the tops of marginally resolved inversions when the vertical velocity is reasonably vertically uniform surrounding the top of the inversion. The Eulerian approximations underestimate the cooling that should occur at the top of the inversion. This is also verified with diagnostic calculations on a grid with substantially increased resolution below 800 mb. On this grid, the adiabatic tendency differences between semi-Lagrangian and Eulerian approximations are small and the two approximations produce the same simulated lower-tropospheric temperature, which is also the same as that produced by the semi-Lagrangian approximations on the coarse grid. Compared to the NCEP reanalysis, the low vertical resolution Eulerian simulated temperature looks better than the semi-Lagrangian, but those approximations produce that ''better'' simulated temperature by an incorrect mechanism. For practical applications, the Eulerian approximations require higher vertical resolution below 800 mb than usually used today in climate models, but the semi-Lagrangian approximations are adequate on these coarser grids.

1. Introduction

The principal advantage that drove the early development of semi-Lagrangian methods was the potential for long time steps. The suitability of long time steps was demonstrated in forecast applications where the forecast was not degraded compared to shorter-time-step Eulerian forecasts. Staniforth and Côté (1991) provide an excellent review of the early development of semi-Lagrangian methods. More recently several other advantages of the semi-Lagrangian approach have been identified. These include the suitability of linear grids with semi-Lagrangian spectral transform models (Côté and Staniforth 1988; Williamson 1997), and two-time-level schemes (McDonald and Bates 1987; Temperton and Staniforth 1987). Linear grids yield a 50% increase in resolution in each horizontal dimension at negligible increased cost. Two-time-level schemes are potentially twice as fast as the more common three-time-level schemes, but in practice that speedup will be only partially realized in complete models because not all the physical parameterizations are calculated every time step.

Semi-Lagrangian approximations have been adopted as the basis of several high-resolution operational numerical weather prediction models (Ritchie and Beaudoin 1994; Ritchie et al. 1995), however, they have not been adopted for the dynamical component of a production atmospheric climate model. Monotonic semi-Lagrangian approximations have been used for the constituent transport component of climate models (Hack et al. 1993; Feichter et al. 1996; Kiehl et al. 1996) but for reasons other than those listed above, namely the property that they produce no over or undershoot in the transported variable (Williamson and Rasch 1989; Rasch and Williamson 1990). The hesitancy of climate modeling centers to replace Eulerian approximations by semi-Lagrangian is partly attributable to the observation that they exacerbate several biases present in matching Eulerian simulations. At the lower vertical resolutions of around 20 levels commonly used in tropospheric climate models, compared to Eulerian approximations the semi-Lagrangian produce a colder tropical tropopause, a warmer polar tropopause, and a colder winter polar lower troposphere (Williamson and Olson 1994; Chen

*The National Center for Atmospheric Research is sponsored by the National Science Foundation.

Corresponding author address: Dr. David L. Williamson, NCAR, P.O. Box 3000, Climate and Global Dynamics Division, Boulder, CO 80307-3000.
E-mail: wmson@ucar.edu

and Bates 1996). The warmer polar tropopause represents an improvement due to the semi-Lagrangian approximations ameliorating a common bias in models (Boer et al. 1992) and is not considered here. The colder tropical tropopause was studied in Williamson et al. (1998) who showed that it resulted from insufficient vertical resolution in the vicinity of the tropopause with the semi-Lagrangian approximations. With increased vertical resolution the semi-Lagrangian approximations create the same tropical temperature structure as the Eulerian at the increased and original resolutions. With both types of approximations, however, the convective parameterization is better behaved with the extra upper-tropospheric resolution, and the tropical temperature bias is reduced compared to the NCEP reanalysis. Thus the extra vertical resolution obviously needed by the semi-Lagrangian approximations is also beneficial to the Eulerian approximations. In this paper we study the nature and cause of the colder polar lower troposphere in the semi-Lagrangian simulations within the framework of the NCAR CCM3. We show that this difference is also due to insufficient vertical resolution, but in this case the Eulerian is the inaccurate approximation. Thus there is no longer any reason not to use semi-Lagrangian approximations as the basis of global atmospheric climate models.

2. Brief description of CCM3

The newest version of the NCAR Community Climate Model, CCM3, was created from the earlier version, CCM2. The model was made more suitable for coupling to land, ocean, and sea–ice models primarily by modifying the subgrid-scale physical parameterizations to reduce the more serious biases observed in CCM2 simulations. The parameterization changes primarily addressed biases in the top-of-atmosphere and surface energy budgets, and included modifications to the representation of radiative transfer through both clear and cloudy atmospheric columns, and modifications to the hydrologic processes modeled in the atmospheric boundary layer and moist convection. A sophisticated land surface model (Bonan 1996) was also included to improve the surface energy exchange.

The radiation and diagnostic cloud changes substantially reduced the systematic biases in the global annually averaged clear-sky and all-sky outgoing longwave radiation and absorbed solar radiation to well within observational uncertainty, while maintaining very good agreement with global observational estimates of cloud forcing. They also reduced the large warm bias in the simulated July surface temperature over the Northern Hemisphere, the systematic overprediction of precipitation over warm land areas, and a large component of the stationary-wave error in CCM2. The changes to the hydrologic processes, primarily in the atmospheric boundary layer and convective parameterizations, produced a substantial reduction in the overall magnitude of the hydrologic cycle and a smoother distribution of tropical precipitation. The annually averaged global latent heat flux and precipitation were reduced by 13% to be closer to values thought to be representative of the atmosphere. These improvements in the radiative and hydrologic cycle characteristics of the model climate were achieved without compromising the quality of the simulated equilibrium thermodynamic structures of CCM2, one of that model's major strengths. While the new parameterizations of CCM3 significantly change the individual simulated climates compared to CCM2, they have little effect on differences between semi-Lagrangian and Eulerian simulated climates when all other aspects of the models being compared are identical.

The changes from CCM2 to CCM3 are summarized in more detail in Kiehl et al. (1996), which also provides complete algorithmic details of the CCM3. An overview of CCM3 is provided in Kiehl et al. (1998a), the simulated energy budget of CCM3 is documented in Kiehl et al. (1998b), the hydrologic and thermodynamic structures simulated by CCM3 are documented in Hack et al. (1998), and Hurrell et al. (1998) document the dynamical aspects of the atmosphere simulated by CCM3.

The parameterizations in the semi-Lagrangian version of CCM3 are identical to those in the Eulerian version summarized above. The numerical approximations of the dynamical component are the semi-Lagrangian approximations developed in Williamson and Olson (1994), modified to eliminate the orographic resonance problem by including the first-order decentering (Rivest et al. 1994) and orographic treatment of Ritchie and Tanguay (1996). Water vapor transport is handled by monotonic semi-Lagrangian approximations in both the Eulerian and semi-Lagrangian versions (Williamson and Rasch 1994). Both models use specified climatological monthly averaged sea surface temperatures and sea-ice distribution at the lower boundary.

In the following we compare simulations from Eulerian and semi-Lagrangian versions of CCM3 with T42 horizontal spectral resolution and a (128×64) quadratic unaliased Gaussian grid. We start with the 26-level grid developed in Williamson et al. (1998). Except where noted, all simulations are for 5 years. Since we are concentrating here on the polar regions, 5-yr averages might be a little short to completely eliminate the natural variability at those latitudes. However, since we consider seasonal averages (December–February) rather than monthly (January), the major signal of concern appears to be above the background noise. The 10-yr standard deviation of the December–February average, zonal average temperature in the standard 18-level Eulerian CCM3 is 1 K at and below 850 mb at 70°N. It decreases equatorward and with increasing height and increases poleward to a value of 2 K at 85°N. The time step for the semi-Lagrangian simulations was held at the 20 min value required by the Eulerian approximations to ensure

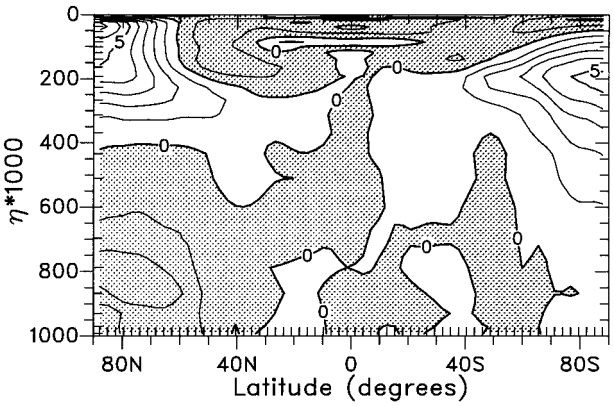

FIG. 1. December–February average, zonal average temperature difference for the 26-level semi-Lagrangian minus Eulerian simulations. Contour interval is 1.0 K, negative regions stippled.

that the parameterizations were not affected by a different time step.

3. Polar lower-troposphere relative cold bias

Figure 1 shows the December–February average, zonal average difference of temperature for the simulations with the 26-level vertical grid. Differences between semi-Lagrangian and Eulerian simulations will always be shown as semi-Lagrangian minus Eulerian. This difference field is comparable to that in Fig. 10 of Williamson et al. (1998), but from different 5-yr simulations. The simulations here started from perturbed initial conditions. The semi-Lagrangian simulation is colder than the Eulerian in the winter polar lower troposphere, with a maximum difference somewhat more than -2 K. The maximum difference in Williamson et al. (1998) was slightly more than -4 K. The semi-Lagrangian simulation contributing to Fig. 1 is warmer than the one in Williamson et al. (1998) by around a degree in the region poleward of 60°N and below 400 mb. The Eulerian simulation here is colder than the previous one in that region by slightly less than a degree. The two combine to yield the 2-K difference between the differences of the simulation pairs (or 1 K in the other possible pairings.) This provides some indication of the natural variability of these 5-yr seasonal averages. This is not inconsistent with the earlier mentioned 1-K, 10-yr standard deviation of seasonal, zonal averages in this region in the 18-level Eulerian CCM3. This variability is small enough that the colder semi-Lagrangian tropospheric signal is robust, although the magnitude itself may vary by 2 K.

In Williamson et al. (1998) we were able to examine the differences between semi-Lagrangian and Eulerian approximations at the tropical tropopause with the Held and Suarez (1994) idealized forcing. Simulations resulting from that forcing showed the same tropopause differences between semi-Lagrangian and Eulerian as those from the complete model. That is not the case with the polar lower-tropospheric signal of concern here.

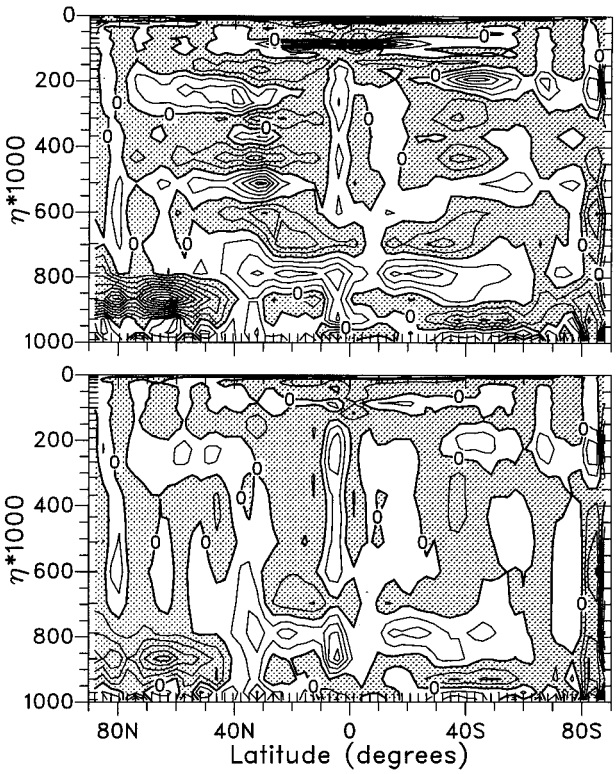

FIG. 2. December–February average, zonal average adiabatic temperature tendency difference for the 26-level simulations, semi-Lagrangian minus Eulerian. Top: Eulerian controls the simulation, semi-Lagrangian is calculated diagnostically; bottom: semi-Lagrangian controls the simulation, Eulerian is calculated diagnostically. Contour interval is 0.1 K day^{-1}, negative regions stippled.

Simulations from the Held and Suarez (1994) idealized forcing do not show a colder polar lower troposphere in the semi-Lagrangian simulations (the reason will become apparent later) and another approach is required to study the cause. It is difficult to separate cause and effect by examining the different balances in the equilibrium simulations produced by each approximation. Therefore we examine the numerical/dynamical component of the models with a diagnostic approach. One set of approximations (semi-Lagrangian or Eulerian) is calculated diagnostically every time step while the other set of approximations (Eulerian or semi-Lagrangian, respectively) combined with the physical parameterizations controls the simulation. Figure 2 shows the December–February average, zonal average adiabatic (dynamical) temperature tendency difference when the Eulerian approximations control the simulation (top) and when the semi-Lagrangian do (bottom). These simulations are only for three years but natural variability is less of an issue in these differences because in either comparison both approximations are based on exactly the same state every time step. The first feature that jumps out is the extratropical vertical grid scale noise in the difference when the Eulerian approximations control the simulation (the grid levels are indicated by the

inner ticks on the left side.) In fact, the noise is in the semi-Lagrangian adiabatic tendency, but it is a result of noise in the state generated by the Eulerian approximations, which the semi-Lagrangian approximations try to remove. Similar noise is not seen in the difference when the semi-Lagrangian approximations control the simulation because it enters the Eulerian system slowly through the forcing and nonlinear interactions. The Eulerian system lacks an effective damping mechanism of these structures leading to the large amplitudes over time.

The dominant signal in the differences occurs poleward of 40°N between 925 and 800 mb, at a single grid level, 860 mb (again, the grid levels are indicated by the inner ticks on the left side). With both control simulations, the semi-Lagrangian dynamics cool relative to the Eulerian, more so with the Eulerian controlled simulation. This is just the region where the temperature difference between the semi-Lagrangian and Eulerian simulations maximizes (Fig. 1), although the colder region extends up to 400 mb, well above the level directly affected by the dynamics. We believe this is the result of the following sequence of processes, for which the differences are described in a relative sense.

Given identical states, the semi-Lagrangian dynamical approximations produce cooling (relative to the Eulerian) at 860 mb (Fig. 2). This destabilizes the lower troposphere and induces increased convection to warm the 860-mb level, but at a somewhat slower rate than the dynamical cooling, and to cool below. This was in fact verified in the diagnostic calculation. The convective clouds increase at 860 mb because the convection increases. The grid-scale clouds increase as well because the relative humidity increases due to the combined effect of increased water vapor at 860 mb resulting from the increased convection and decreased temperature from the numerical approximations. The radiative heating increases below the increased clouds and compensates the increased convective cooling there. The radiative cooling increases in and above the increased clouds and ultimately spreads the relative cooling and increased clouds upwards through the troposphere to 400 mb. As the troposphere cools, the clouds increase throughout the region leading to more radiative cooling there. In the final equilibrium states, the increased radiative cooling associated with the increased clouds is balanced by decreased radiative cooling associated with the colder temperatures, and the only difference in the radiation heating is at 925 mb below the increased clouds. This heating balances the increased convective cooling there. The energy source for the increased convection comes from increased fluxes from the surface.

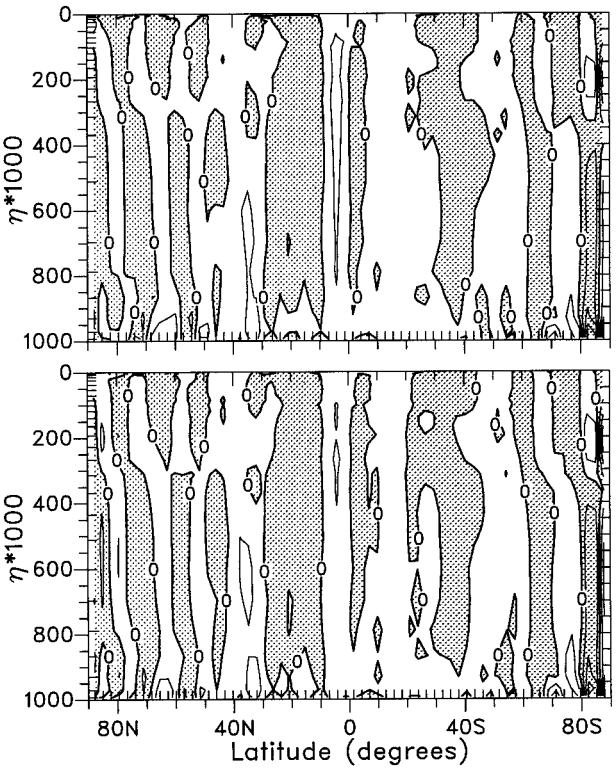

FIG. 3. December–February average, zonal average adiabatic temperature tendency difference for the 26-level simulations, NIIV semi-Lagrangian minus Eulerian. Top: Eulerian controls the simulation, NIIV semi-Lagrangian is calculated diagnostically; bottom: NIIV semi-Lagrangian controls the simulation, Eulerian is calculated diagnostically. Contour interval is 0.1 K day^{-1}, negative regions stippled.

4. Noninterpolating-in-the-vertical semi-Lagrangian simulations

Whatever the final climate balance, the ultimate cause of the differences is the numerical approximations, the only component changed. The question remains as to what is responsible for the difference and which approximations offer more accurate representations of the process in the atmosphere being modeled. Because the differences in the adiabatic temperature tendencies are concentrated at one vertical grid point (Fig. 2) one naturally suspects they are due to the vertical approximations rather than the horizontal. To establish this we carried out similar diagnostic calculations with Eulerian and noninterpolating-in-the-vertical (NIIV) semi-Lagrangian approximations (Ritchie 1991). Because we use a 20-min time step for all the simulations reported here, the Courant number remains below 1 and this system is essentially Eulerian in the vertical and identical in the vertical to the approximations in the three-dimensional Eulerian system. It remains semi-Lagrangian in the horizontal. Figure 3 shows the December–February average, zonal average adiabatic temperature tendency difference when the Eulerian approximations control the simulation (top) and when the NIIV semi-Lagrangian do (bottom). Again, the diagnostic calculation is for three winters. Except for a small amount of spectral noise, the approximations are the same. In fact the simulated lower-tropospheric temperature produced by

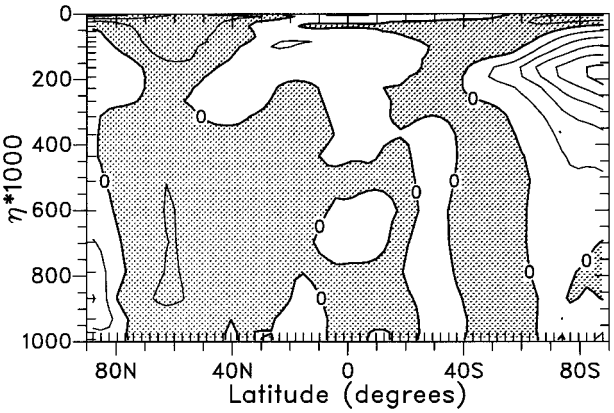

FIG. 4. December–February average, zonal average temperature difference for the 26-level NIIV semi-Lagrangian minus Eulerian simulations. Contour interval is 1.0 K, negative regions stippled.

the semi-Lagrangian and Eulerian approximations are also the same. This is seen in Fig. 4 which shows the zonal average temperature difference averaged over five winters. Below 400 mb, the simulations match to within the natural variability. The NIIV semi-Lagrangian produces a warmer summer polar tropopause than the Eulerian. This signal has been consistently seen in semi-Lagrangian and Eulerian comparisons. Surprisingly, a similar signal is not seen at the winter polar tropopause, but there the bias in the Eulerian simulation is smaller to start with. A similar comparison of 18-level simulations (not shown) also shows no difference in the winter polar tropopause temperature and only a 2-K difference in the summer polar tropopause, NIIV semi-Lagrangian again being warmer.

5. 36-level simulations

We conclude from the Eulerian and NIIV semi-Lagrangian comparison that the cold polar lower-troposphere relative bias in the (three-dimensional interpolating) semi-Lagrangian simulation is due to the vertical advection component of the approximations. Since the dynamical signal is predominantly at a single vertical grid level (Fig. 2), we also surmise that it is related to vertical resolution. To determine if this is the case, we repeated the diagnostic calculations with the semi-Lagrangian and Eulerian approximations using 36 levels with substantially increased resolution below 800 mb. In this grid the interval gradually increases from 15 mb at the surface to 26 mb at 800 mb, then increases more rapidly up to 250 mb where the levels become very similar to those of the 26-level grid. The actual details of the parameters determining the grid are presented in Table 1. The algorithm to which they apply is described in appendix B of Williamson et al. (1998). The locations of the midlayers are illustrated in Fig. 5 for the 26- and 36-level grids. The original 18-layer CCM3 grid is also shown for comparison.

TABLE 1. Grid generation parameters.

	Top	Increment	Maximum
26-layer grid Surface-layer thickness = 0.015			
Boundary layer	970	0.015	1.0
Troposphere	90	0.0267	0.1625
Lower stratosphere	40	0.08	1.0
Middle stratosphere	3	0.1	1.0
36-layer grid Surface-layer thickness = 0.015			
Boundary layer	800	0.002	1.0
Lower troposphere	600	0.0085	0.1625
Upper troposphere	90	0.0125	0.1625
Lower stratosphere	40	0.08	1.0
Middle stratosphere	3	0.1	1.0

The adiabatic temperature tendency difference is shown in Fig. 6 for this 36-level grid. Again, the top panel shows the difference when the Eulerian approximations control the simulation and the bottom when the semi-Lagrangian do. These differences are small compared to those in Fig. 2 for the 26-level case. With the 36-level grid the two approximations produce very similar dynamical tendencies. This is reflected in the difference of the temperature field between the semi-Lagrangian and Eulerian simulations shown in Fig. 7. Except at the polar tropopause in both hemispheres, the temperature differences are small, and inseparable from the natural variability.

Returning to Fig. 6, two regions with small vertical scale differences in the adiabatic temperature tendency difference stand out. One, poleward of 50°N and near the surface will be discussed later. The other is between 40°N and 40°S around 800 mb. This structure arises where the vertical grid interval first increases more rapidly with height. It arises because each approximation tends to change the equilibrium temperature structure created by the other to a state consistent with itself. In the top panel, the semi-Lagrangian approximations work to smooth a grid-scale structure created by the Eulerian

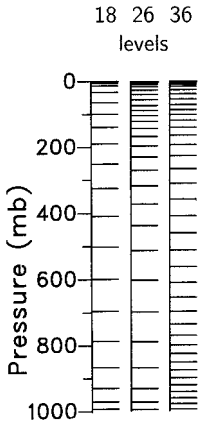

FIG. 5. The 18-, 26- and 36-layer grids. Bars indicate midlayers where *u, v, T,* and *q* are calculated.

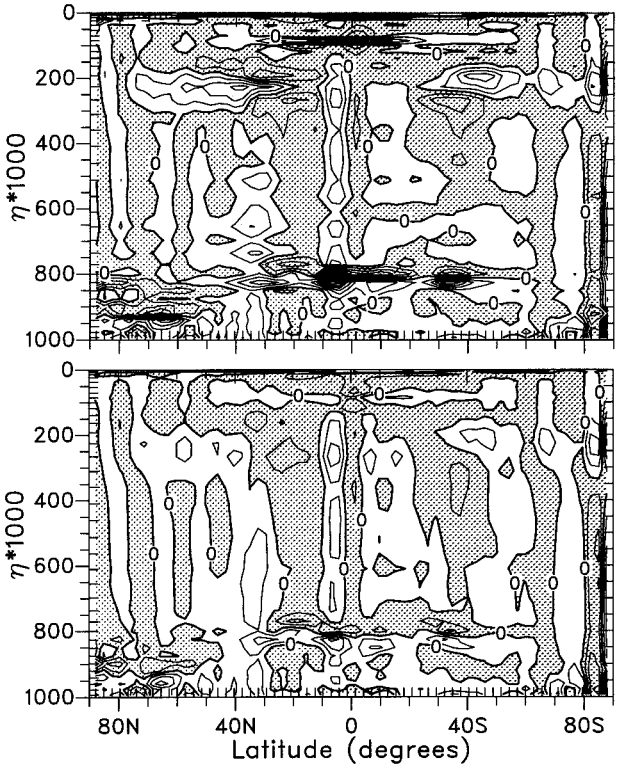

FIG. 6. December–February average, zonal average adiabatic temperature tendency difference for the 36-level simulations, semi-Lagrangian minus Eulerian. Top: Eulerian controls the simulation, semi-Lagrangian is calculated diagnostically; bottom: semi-Lagrangian controls the simulation, Eulerian is calculated diagnostically. Contour interval is 0.1 K day^{-1}, negative regions stippled.

at the grid discontinuity; in the bottom, the Eulerian tends to introduce noise structures into the slightly smoother structure created by the semi-Lagrangian. The differences in the structures are small and difficult to see in the temperature fields themselves. Earlier, we had performed a diagnostic calculation (not shown) with a grid which was even finer from 1000 to 800 mb, then became much coarser above 800 mb, closer there to the grid structure in the 26-level grid. With this discontinuity in the vertical grid interval, the grid-scale structure in the difference of the adiabatic temperature tendency was extremely strong surrounding 800 mb where the grid interval changed abruptly. In that case, grid-scale kinks were visible in the contours of the Eulerian zonal averaged temperature around 800 mb, but were not visible in the semi-Lagrangian. This provides another example where the Eulerian approximations tend to produce a noisier field with more grid-scale structures than the semi-Lagrangian. The inherent smoothing in the semi-Lagrangian approximations produce a slightly smoother field.

6. Cause of differences

While the above analysis indicates that the two approximations produce the same simulation at sufficiently

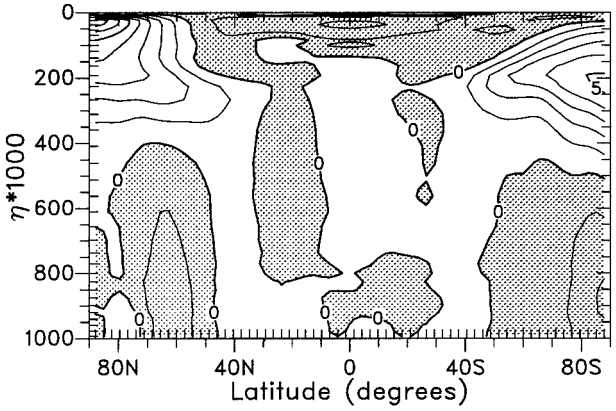

FIG. 7. December–February average, zonal average temperature difference for the 36-level semi-Lagrangian minus Eulerian simulations. Contour interval is 1.0 K, negative regions stippled.

high vertical resolution, it is of interest to determine which is more accurate at the lower resolution and what is the nature of the error in the other. To determine this we first establish where the difference primarily occurs. Figure 8 shows the adiabatic temperature tendency dif-

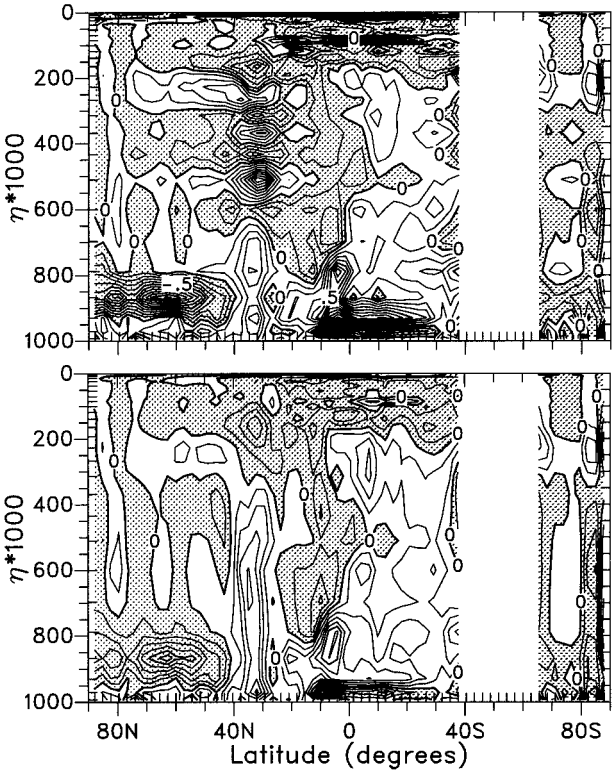

FIG. 8. December–February average, zonal average adiabatic temperature tendency difference for the 26-level simulations, semi-Lagrangian minus Eulerian, averaged over land and sea ice. Top: Eulerian controls the simulation, semi-Lagrangian is calculated diagnostically; bottom: semi-Lagrangian controls the simulation, Eulerian is calculated diagnostically. Contour interval is 0.1 K day^{-1}, negative regions stippled.

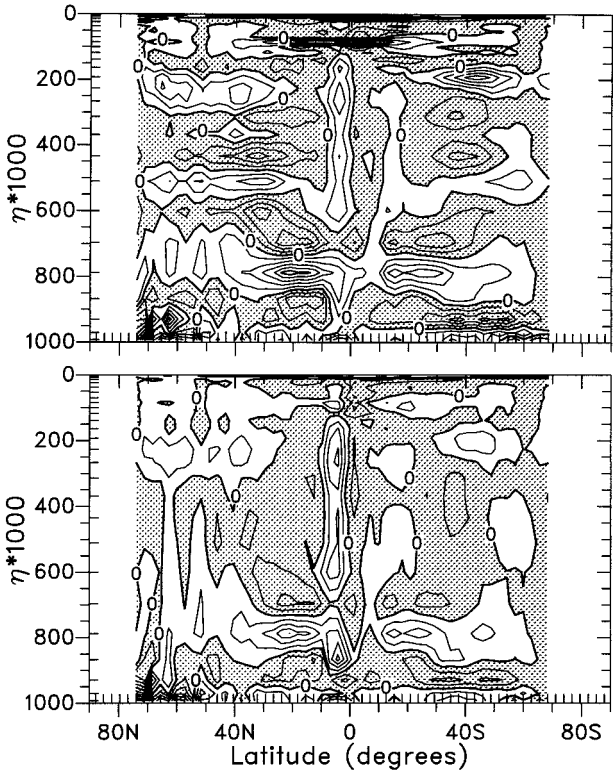

FIG. 9. December–February average, zonal average adiabatic temperature tendency difference for the 26-level simulations, semi-Lagrangian minus Eulerian, averaged over ocean. Top: Eulerian controls the simulation, semi-Lagrangian is calculated diagnostically; bottom: semi-Lagrangian controls the simulation, Eulerian is calculated diagnostically. Contour interval is 0.1 K day^{-1}, negative regions stippled.

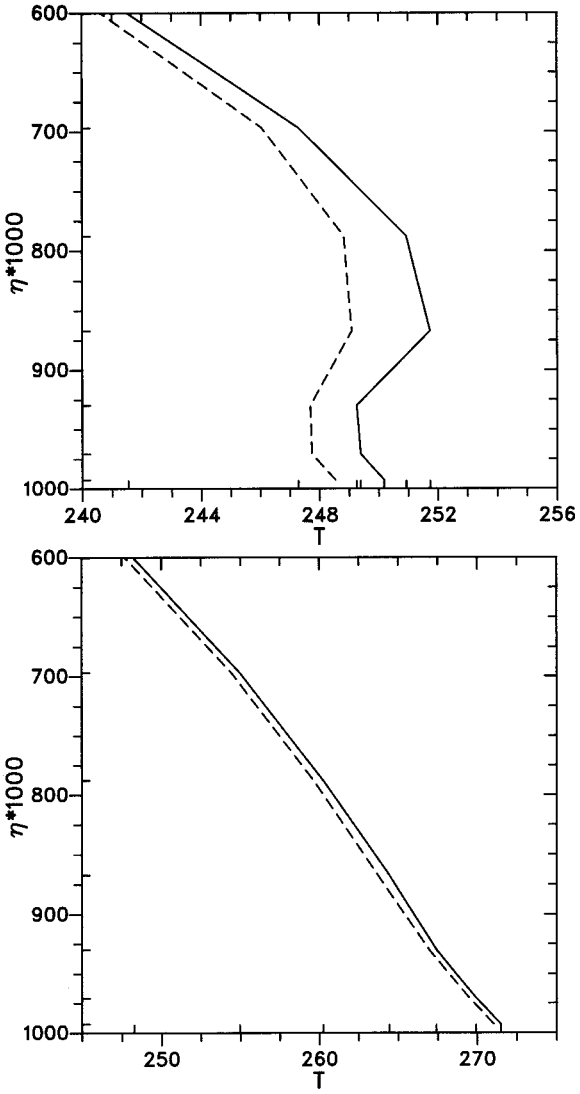

FIG. 10. December–February average, zonal average temperature profiles for the 26-level simulations averaged from 55° to 90°N, averaged over land and sea ice (top) and averaged over oceans (bottom). Solid line is Eulerian and dashed is semi-Lagrangian.

ferences for the 26-level simulations averaged over land and sea ice, and Fig. 9 shows them averaged over ocean. The polar tendency differences occur over land and sea ice, and not over the oceans. Figure 10 shows the zonal average temperature profiles in the polar region for the 26-level simulations averaged over land and sea ice (top) and averaged over the ocean (bottom) for the Eulerian (solid) and semi-Lagrangian (dashed) simulations. In the polar region the vertical temperature structures are very different over land and sea ice than over ocean. Over ocean, where the surface temperatures are specified by climatological monthly averaged values, the atmospheric temperature decreases monotonically with height. Over land and sea ice, where the surface temperature is calculated prognostically with land and sea-ice models, an inversion forms in the atmosphere with its top at the 860-mb grid level. The inversion is slightly stronger in the Eulerian simulation. The semi-Lagrangian and Eulerian approximations treat this structure differently. In CCM3 the Eulerian vertical advection approximation is derived on a grid with vertical velocity staggered between temperature levels. It has the form

$$\dot{\eta}\frac{\partial p}{\partial \eta}\frac{\partial T}{\partial p} = \frac{1}{2\Delta p_k}\left[\left(\dot{\eta}\frac{\partial p}{\partial \eta}\right)_{k+1/2}(T_{k+1} - T_k) + \left(\dot{\eta}\frac{\partial p}{\partial \eta}\right)_{k-1/2}(T_k - T_{k-1})\right],$$

where k is the vertical grid index, T is temperature, p is pressure, η is the hybrid vertical coordinate, and $\dot{\eta}$ is the hybrid system vertical velocity. Consider an idealized case of a symmetric temperature structure about the top of the inversion, uniform vertical grid interval, and uniform vertical motion in the column, either upward or downward. Then

$$T_{k+1} - T_k = -(T_k - T_{k-1}),$$

$$\left(\dot{\eta}\frac{\partial p}{\partial \eta}\right)_{k+1/2} = \left(\dot{\eta}\frac{\partial p}{\partial \eta}\right)_{k-1/2},$$

and

$$\dot{\eta}\frac{\partial p}{\partial \eta}\frac{\partial T}{\partial p} = 0.$$

In this special case, the Eulerian vertical advection is zero at the top of the inversion. Note that this is incorrect and the structure should be displaced by the dynamics alone. The semi-Lagrangian vertical advection will not be zero there. The semi-Lagrangian vertical advection alone can be written as

$$T_k^{n+1} = L_\eta(T^{n-1}),$$

where n denotes the time level of the data, and L_η denotes the semi-Lagrangian interpolation to the vertical departure point. In this idealized symmetric case with nonzero vertical motion, this interpolated value will be between T_k and $T_{k\pm1}$, and the semi-Lagrangian advection approximations cool the top of the inversion with either upward or downward vertical motion. Of course, the simulated model structures are not as simple as this symmetric case used for illustration, but this example provides a relevant description for a significant component of the simulation case. The zonal average simulated vertical motion (not shown) is reasonably vertically uniform surrounding the top of the inversion. Because of the staggered vertical grid, the Eulerian approximations will not erode the top of the inversion as fast as they should and the semi-Lagrangian approximations provide a better representation of this phenomenon. This also explains why the inversion is somewhat stronger in the Eulerian simulation than in the semi-Lagrangian (Fig. 10), and why the semi-Lagrangian cools relatively more in the Eulerian controlled simulation than in the semi-Lagrangian controlled simulation (Figs. 2 and 8). In the Eulerian produced state, the top of the inversion is sharper than in the semi-Lagrangian produced state and the semi-Lagrangian approximations will produce a larger relative change with the Eulerian state. On the other hand, to a large extent the Eulerian approximations do not see the top of the inversion in either state. The different character of the approximations also explains why some grid-scale structures remain in the 36-level difference near the surface in the polar regions (Fig. 6). In this case they are associated with the base of the inversion which has grid-scale structure. The top is more smoothly defined.

One additional indication that the semi-Lagrangian is more accurate and produces a state closer to the 36-level simulations is provided by the temperature difference between the 26- and 36-level simulations shown in Fig. 11. The 26-level Eulerian simulation is 3 K warmer than the 36-level Eulerian in the polar region

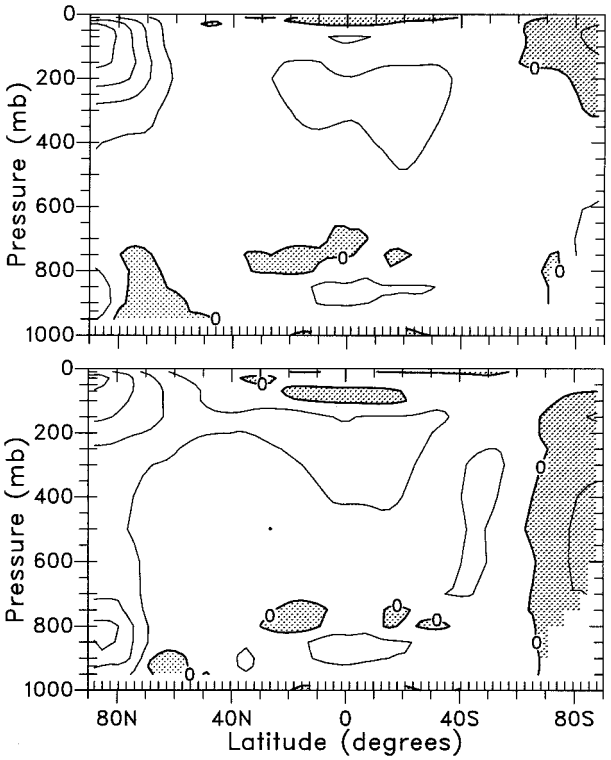

FIG. 11. December–February average, zonal average temperature difference, 26-level minus 36-level simulations for semi-Lagrangian (top) and Eulerian (bottom). Contour interval is 1.0 K, negative regions stippled.

while the semi-Lagrangian is only 1 K warmer right at the pole. Also, recall that the 26-level Eulerian simulation was 2 K warmer than the semi-Lagrangian there (Fig. 1). The warmer region, however, extends farther equatorward than the difference in the lower panel of Fig. 11. This is a reflection of the difference in the temperature fields (Fig. 7), which shows the 36-level semi-Lagrangian colder by around 1 K at 60°N. The 1-K magnitude of these differences is enough to require very long runs to remove the contamination of the signal by the natural variability. We believe further refinement of these experiments is not worth the computational expense. The primary signal between the approximations seems clear enough.

Finally, Fig. 12 shows the zonal average difference of the 36-level semi-Lagrangian simulation with the NCEP reanalysis (top) and 36-level Eulerian minus NCEP reanalysis (bottom) for December–February averages. As expected from the temperature difference between the two simulations (Fig. 7) the differences with the NCEP reanalysis are very similar except at the polar tropopause. The 36-level simulations are slightly colder in the tropical troposphere than the 26-level ones, thus the temperature biases in the 36-level simulations are negative throughout the tropical troposphere, whereas the 26-level simulations (Fig. 11 of Williamson et al. 1998) varied from slightly positive to slightly negative

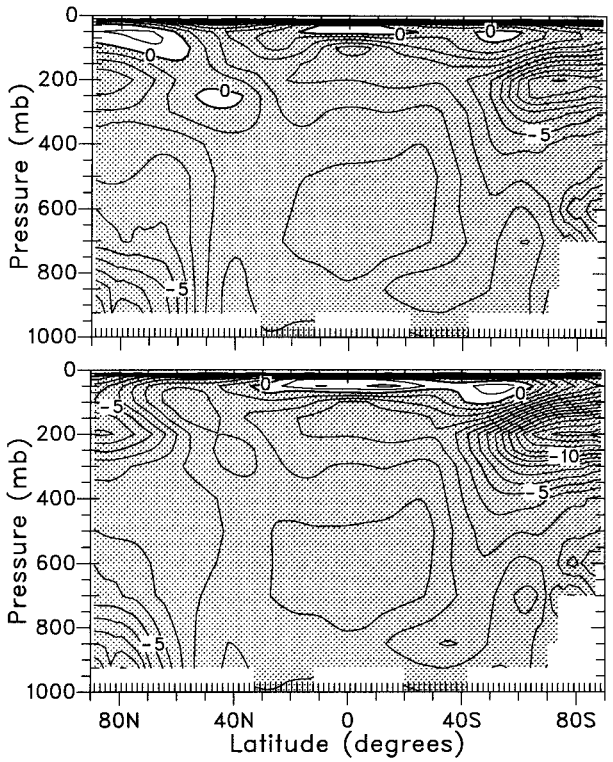

FIG. 12. December–February average, zonal average temperature difference for 36-level model minus NCEP reanalysis, semi-Lagrangian (top) and Eulerian (bottom). Contour interval is 1.0 K, negative regions stippled.

there. The only significant differences remaining between the Eulerian and semi-Lagrangian simulations are the warmer polar tropopause in the semi-Lagrangian. These represent a significant decrease in the model biases in those regions in the semi-Lagrangian simulation.

7. Conclusions

We examine the differences in the polar lower-tropospheric temperature simulated by semi-Lagrangian and Eulerian approximations and identify their source. With the standard 18-level CCM3 grid and the 26-level grid developed to improve the tropical tropopause simulation, semi-Lagrangian simulations are colder than Eulerian by 2–4 K in the region poleward of 60°N and below 400 mb in winter. These two grids have 8–10 layers below 500 mb. The temperature difference is primarily centered around the grid level at 860 mb. With diagnostic calculations we show that the semi-Lagrangian dynamical approximations tend to produce a cooling relative to the Eulerian at the 860-mb level. The difference occurs over land and sea ice, both of which are represented by prognostic models. The difference does not occur over oceans where the surface temperature is specified as climatological monthly averages. Over ocean the atmospheric temperature decreases monotonically with height; over land and sea ice an inversion forms in the atmosphere with its top around the 860-mb grid level. By contrasting diagnostic calculations from noninterpolating-in-the-vertical semi-Lagrangian approximations with three-dimensional interpolating semi-Lagrangian approximations the source of the relative cooling was isolated in the vertical component of the approximations. The NIIV approximations are essentially Eulerian in the vertical and identical to the vertical approximations in the three-dimensional Eulerian system. They remain semi-Lagrangian in the horizontal. The source of the difference was found to be the different way the vertical advection approximations treat vertical structures found at the tops of marginally resolved inversions when the vertical velocity is reasonably vertically uniform surrounding the top of the inversion. With a staggered vertical grid as in CCM3, the Eulerian advection is calculated as an average of discrete advection terms evaluated above and below the top of the inversion, where the temperature gradients are opposite. These tend to cancel and the Eulerian approximations do not erode the top of the inversion as fast as they should. The semi-Lagrangian approximations provide a better representation of this phenomenon.

This was further verified by performing diagnostic calculations with increased resolution below 800 mb. A 36-level grid was used that had substantially increased resolution there. On this grid, the adiabatic tendency differences between semi-Lagrangian and Eulerian approximations are small. In addition, the two sets of approximations produce the same simulated lower-tropospheric temperature on the 36-level grid. The 26-level semi-Lagrangian simulation is closer to these 36-level simulations than the Eulerian is. Compared to the NCEP reanalysis, these two 36-level simulations and the 26-level semi-Lagrangian simulation show a stronger polar lower-troposphere cold bias. The 26-level Eulerian simulation is actually closer to the NCEP reanalysis, but it produces this ''better'' simulation by an incorrect mechanism. Therefore, for practical applications, the Eulerian approximations require higher vertical resolution below 800 mb than usually used in climate models today, but the semi-Lagrangian approximations are adequate on these coarser grids.

Acknowledgments. We would like to thank Byron Boville and Philip Rasch for helpful comments on the original manuscript. This work was partially supported by the Computer Hardware, Advanced Mathematics, and Model Physics (CHAMMP) Program, which is administered by the Office of Energy Research under the Office of Health and Environmental Research in the U.S. Department of Energy, Environmental Sciences Division.

REFERENCES

Boer, G. J., and Coauthors, 1992: Some results from an intercomparison of the climates simulated by 14 atmospheric general circulation models. *J. Geophys. Res.,* **97,** 12 771–12 786.

Bonan, G. B., 1996: A land surface model (LSM version 1.0) for ecological, hydrological, and atmospheric studies: Technical description and user's guide. NCAR Tech. Note NCAR/TN-417+STR, National Center for Atmospheric Research, Boulder, CO, 150 pp.

Chen, M., and J. R. Bates, 1996: A comparison of climate simulations from a semi-Lagrangian and an Eulerian GCM. *J. Climate,* **9,** 1126–1149.

Côté, J., and A. Staniforth, 1988: A two-time-level semi-Lagrangian semi-implicit scheme for spectral models. *Mon. Wea. Rev.,* **116,** 2003–2012.

Feichter, J., E. Kjellström, H. Rodhe, F. Dentener, J. Lelieveld, and G.-J. Roelofs, 1996: Simulation of the tropospheric sulfur cycle in a global climate model. *Atmos. Environ.,* **30,** 1693–1707.

Hack, J. J., J. T. Kiehl, and J. W. Hurrell, 1998: The hydrologic and thermodynamic structure of the NCAR CCM3. *J. Climate,* in press.

——, B. A. Boville, B. P. Briegleb, J. T. Kiehl, P. J. Rasch, and D. L. Williamson, 1993: Description of the NCAR Community Climate Model (CCM2). NCAR Tech. Note NCAR/TN-382+STR, Boulder, CO, 108 pp.

Held, I. M., and M. J. Suarez, 1994: A proposal for the intercomparison of the dynamical cores of atmospheric general circulation models. *Bull. Amer. Meteor. Soc.,* **75,** 1825–1830.

Hurrell, J. W., J. J. Hack, B. A. Boville, D. L. Williamson, and J. T. Kiehl, 1998: The dynamical simulation of the NCAR CCM3. *J. Climate,* in press.

Kiehl, J. T., J. J. Hack, G. B. Bonan, B. A. Boville, B. P. Briegleb, D. L. Williamson, and P. J. Rasch, 1996: Description of the NCAR Community Climate Model (CCM3). NCAR Tech. Note NCAR/TN-420+STR, Boulder, CO, 152 pp.

——, ——, ——, ——, D. L. Williamson, and P. J. Rasch, 1998a: The National Center for Atmospheric Research Community Climate Model: CCM3. *J. Climate,* in press.

——, J. J. Hack, and J. W. Hurrell, 1998b: The energy budget of the NCAR Community Climate Model: CCM3. *J. Climate,* in press.

McDonald, A., and J. R. Bates, 1987: Improving the estimate of the departure point position in a two-time level semi-Lagrangian and semi-implicit scheme. *Mon. Wea. Rev.,* **115,** 737–739.

Rasch, P. J., and D. L. Williamson, 1990: On shape-preserving interpolation and semi-Lagrangian transport. *SIAM J. Sci. Stat. Comput.* **11,** 656–687.

Ritchie, H., 1991: Application of the semi-Lagrangian method to a multilevel spectral primitive-equations model. *Quart. J. Roy. Meteor. Soc.,* **117,** 91–106.

——, and C. Beaudoin, 1994: Approximations and sensitivity experiments with a baroclinic semi-Lagrangian spectral model. *Mon. Wea. Rev.,* **122,** 2391–2399.

——, and M. Tanguay, 1996: A comparison of spatially averaged Eulerian and semi-Lagrangian treatments of mountains. *Mon. Wea. Rev.,* **124,** 167–181.

——, C. Temperton, A. Simmons, M. Hortal, T. Davies, D. Dent, and M. Hamrud, 1995: Implementation of the semi-Lagrangian method in a high-resolution version of the ECMWF forecast model. *Mon. Wea. Rev.,* **123,** 489–514.

Rivest, C., A. Staniforth, and A. Robert, 1994: Spurious resonant response of semi-Lagrangian discretizations to orographic forcing: Diagnosis and solution. *Mon. Wea. Rev.,* **122,** 366–376.

Staniforth, A., and J. Côté, 1991: Semi-Lagrangian integration schemes for atmospheric models—A review. *Mon. Wea. Rev.,* **119,** 2206–2223.

Temperton, C., and A. Staniforth, 1987: An efficient two-time-level semi-Lagrangian semi-implicit integration scheme. *Quart. J. Roy. Meteor. Soc.,* **113,** 1025–1039.

Williamson, D. L., 1997: Climate simulations with a spectral, semi-Lagrangian model with linear grids. *Numerical Methods in Atmospheric and Oceanic Modeling. The André J. Robert Memorial* Volume, C. Lin, R. Laprise, and H. Ritchie, Eds., 279–292.

——, and P. J. Rasch, 1989: Two-dimensional semi-Lagrangian transport with shape-preserving interpolation. *Mon. Wea. Rev.,* **117,** 102–129.

——, and J. G. Olson, 1994: Climate simulations with a semi-Lagrangian version of the NCAR Community Climate Model. *Mon. Wea. Rev.,* **122,** 1594–1610.

——, and P. J. Rasch, 1994: Water vapor transport in the NCAR CCM2. *Tellus,* **46A,** 34–51.

——, J. G. Olson, and B. A. Boville, 1998: A comparison of semi-Lagrangian and Eulerian tropical climate simulations. *Mon. Wea. Rev.,* **126,** 1001–1012.